Diffusion of particles bouncing on a one-dimensional periodically corrugated floor

Takahisa Harayama
ATR Adaptive Communications Research Laboratories, 2-2 Hikaridai, Seika-cho, Soraku-gun, Kyoto 619-02, Japan

Pierre Gaspard
Center for Nonlinear Phenomena and Complex Systems, Université Libre de Bruxelles, Campus Plaine, Code Postal 231, Boulevard du Triomphe, B-1050 Brussels, Belgium

(Received 1 March 2001; published 28 August 2001)

We report on a class of spatially extended mechanical systems sustaining a transport process of diffusive type. These systems consist of a point particle subject to a constant vertical acceleration and bouncing on a one-dimensional periodically corrugated floor. We show that the deterministic dynamics of these systems is chaotic with small elliptic islands for many parameter values. The motion of particles perturbed by a small noise has a horizontal diffusion that is normal. In such a case, we show that the diffusion coefficient oscillates periodically as the energy of particles increases. In the absence of noise, there still exists an effective numerical value for the diffusion coefficient and this value has an irregular dependence on energy.

DOI: 10.1103/PhysRevE.64.036215 PACS number(s): 05.45.Ac, 05.40.Fb, 05.60.Cd, 72.10.Bg

I. INTRODUCTION

In recent years, dynamical chaos has been at the center of the preoccupations in our understanding of transport properties in nonequilibrium statistical mechanics. The compatibility of the phenomenological time-irreversible diffusion equation with those of time-reversible Hamiltonian dynamics that shows hyperbolicity has been much discussed. Bunimovich and Sinai have proved that the motion of a particle in the periodic Lorentz gas with a finite horizon follows a Brownian motion in a certain scaling limit [1]. Gaspard and Nicolis have derived an escape-rate formula that connects the diffusion coefficients with the chaotic dynamical properties [2]. Morever, the Pollicott-Ruelle resonances were proved to approach to the eigenvalues of the phenomenological diffusion equation in the case of the multibaker mapping [3]. More recently, the hydrodynamic modes of diffusion associated with these Pollicott-Ruelle resonances have been shown to display a fractal structure in the cases of the multibaker mapping and two hyperbolic Lorentz gases [4,5]. Besides, the transport coefficients and the reaction rates can have an irregular fractal-like dependence on the control parameters of the system. This result has been established by Klages and Dorfman for the case of one-dimensional piecewise-linear mappings [6–9]. These works show that the deterministic chaotic dynamics induces irregular fractal-like structures that were previously unexpected among the transport properties.

Transport by diffusion has also been studied in nonhyperbolic chaotic dynamical systems. Systems that are area preserving are known to present complicated phase portraits with regular motion in the form of elliptic islands coexisting with chaotic one. A famous example is the standard map that has been studied as a paradigm of diffusive transport in Hamiltonian systems with two degrees of freedom. These studies have shown that elliptic islands generate anomalous diffusion with long-time tail effects, preventing the existence of a positive and finite diffusion coefficient. Therefore, a normal diffusion cannot be expected in the presence of elliptic islands.

However, small elliptic islands corresponding to regular motions can be easily destroyed by small noises. In this way, Rechester and White have shown that a system, such as the standard map, which is not fully chaotic can have normal diffusions when perturbed by small noises [10]. The resulting diffusion coefficient is largely independent of the amplitude of a weak noise so that the diffusion is essentially induced by the chaotic dynamics of the system without noise. Moreover, Rechester and White have shown that the effective diffusion coefficient of the standard map presents an oscillatory dependence on the system [10]. It turns out that an effective diffusion coefficient can still be numerically obtained for many parameter values in nonhyperbolic chaotic systems.

On the other hand, our investigations will show that, even if the parameter values where elliptic islands exist could be dense, the measure of the parameter values for which no elliptic island exists may still be positive in our systems. Accordingly, we may wonder if the transport properties in nonhyperbolic systems could not be reminiscent in many respects to the ones in hyperbolic systems.

The purpose of this article is to investigate this problem by considering diffusive transport in mechanical systems such as billiards in an external field. The systems we consider are composed of a particle flying in a vertical constant electric or gravitational field and bouncing elastically on a periodically corrugated wall that extends horizontally.

The class of billiard systems we introduce here differs from conventional billiards on the plane, especially, in that the dynamical properties have a nontrivial dependence on energy. In particular, we show that the diffusion coefficient has an oscillatory dependence on energy, which is reminiscent of the behavior observed in the standard map by Rechester and White.

Besides, we show that these systems are not fully chaotic because there exist many parameter values for which very small elliptic islands corresponding to regular motion coexist in the phase space with chaotic motion. However, these very small elliptic islands are easily destroyed by a weak noise. In this case, the chaotic motion and the weak noise induces a normal diffusion of the particles. This diffusion is normal in the sense that the horizontal displacement of the particle has asymptotically a Gaussian distribution at long times. More-

over, we observe that the diffusion coefficient in presence of a weak noise has a value that is very close to the effective diffusion coefficient computed numerically in absence of noise. Switching off the noise reveals an irregular—but reproducible—dependence of the effective diffusion coefficient on the energy. This phenomenon has similarities with the fractal-like behavior of the diffusion coefficient, as reported for one-dimensional mappings by Klages and Dorfman [6].

This paper is composed of ten sections. In Sec. II, we introduce the mechanical systems of the billiard with a vertical constant acceleration. The linear stability analysis is described in Sec. III, and it plays an important role to obtain the phase diagram as shown in Sec. IV.

In Sec. V, we show that a diffusive type of transport exists in the system. The calculation of the diffusion coefficient is expressed in terms of the velocity autocorrelation function. The autocorrelation function decay algebraically in the region of energy where elliptic periodic orbits exist. In the energy ranges where no islands can be detected numerically, the diffusion coefficient is shown to be an irregular function of energy.

In Sec. VI, we discuss the case that the system is perturbed by a weak noise, the decay of the correlation function is of exponential type and, hence, the diffusion is normal because the small islands are destroyed by the weak noise. The oscillatory dependence of the diffusion coefficient on energy is shown.

In the case of the infinite radius of the curvature of the billiard wall, we show the existence of an invariant Cantor-like subset of chaotic motion in Sec. VII.

In Sec. VIII, we introduce a different billiard with a sawtoothlike floor in order to elucidate the unique behavior of the oscillatory dependence of the diffusion coefficient evidenced in Sec. VI, as well as the irregular behavior of the diffusion coefficient described in Sec. V.

Summary and conclusions are drawn in Sec. IX, where we also discuss the possible experimental application of the results of Sec. VI.

II. THE BILLIARD WITH A VERTICAL CONSTANT ACCELERATION

The class of billiards we consider are composed of a point particle of mass m moving in a constant vertical acceleration g so that its Hamiltonian is

$$H=\frac{1}{2m}p_x^2+\frac{1}{2m}p_y^2+mgy, \tag{1}$$

where x and y denote the horizontal and vertical coordinates of position, respectively, while p_x and p_y are the corresponding momenta. The point particle undergoes elastic collisions on the floor. The shape of the floor is given by the function

$$y=h(x)=h(x+1), \tag{2}$$

which is periodic in the horizontal direction x and has a piecewise-continuous second derivative. Therefore, the floor consists of copies of a fundamental tile, as shown in Fig. 1.

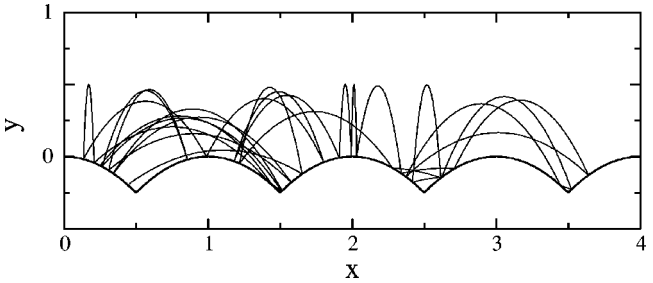

FIG. 1. The spatially extended billiard composed of a point particle moving in a downward vertical field and bouncing on a periodically corrugated floor. The floor is made of arcs of parabolas intersecting at right angle ($r=1/2$). In our case, $m=1$ and $g=15$.

If the energy is very small, the point particle is confined in one of the holes in the floor. The dynamical properties of the point particle in such holes is reminiscent of the ''wedge billiards'' that consist of two flat walls intersecting with each other at the bottom and that have been studied in detail both numerically and analytically [11,12].

If the energy is high enough, the point particle can jump over the top of each tile and wander on the floor by bouncing back and forth.

In general, we can reduce the continuous time flow of our system to a two-dimensional mapping called the Poincaré-Birkhoff mapping that rules the time evolution from collision to collision. This mapping is area preserving in the so-called Birkhoff coordinates $\mathbf{z}=(s,v)$, which are the arc of perimeter s and the component of velocity v that is tangent to the wall, both taken at the point of impact reported to the fundamental tile of the lattice. With such a Poincaré-Birkhoff construction, the flow can be shown to be completely equivalent to the iteration [13,14]:

$$\begin{aligned}\mathbf{z}_{n+1}&=\mathbf{f}(\mathbf{z}_n),\\ t_{n+1}&=t_n+\tau(\mathbf{z}_n),\\ l_{n+1}&=l_n+a(\mathbf{z}_n),\end{aligned} \tag{3}$$

where the first equation gives the Poincaré-Birkhoff mapping itself, and where the second equation gives the successive times $\{t_n\}$ of collision if $\tau(\mathbf{z})$ is the time of flight between two successive collisions. In the third equation of Eq. (3), $a(\mathbf{z})$ is an integer depending on the previous collision and giving the signed number of tiles the particle has jumped over during its flight. $a(\mathbf{z})$ is positive (negative) if the particle jumps to the right (left). The collisional dynamics of the particle can thus be expressed as the successive iterations of this Poincaré-Birkhoff mapping.

III. LOCAL LYAPUNOV EXPONENTS

The vertical components of position and momentum of the particle are convenient to study billiards in a vertical external field, instead of the components perpendicular to the orbit as commonly used in the case of plane billiards, because the vertical acceleration breaks the isotropy of the motion. In these vertical components, the mapping can be linearized and written as a matrix. The dynamical instability can be characterized by the Lyapunov exponent that is the rate of exponential separation between trajectories issued

from arbitrarily close initial conditions. We can show that the Lyapunov exponent λ is given by

$$\lambda = \lim_{N\to\infty} \frac{1}{T_N} \sum_{n=1}^{N} \ln \left| \left(1 - \frac{m^2 g^2 \tau_{n-1}^2}{p_{n-1}^2} \right) + \tau_{n-1} \frac{p_{n-1}^2 + p_n^2 - m^2 g^2 \tau_{n-1}^2}{2 p_{n-1}^2} B_v^{(+)}(n-1) \right|, \quad (4)$$

where $T_N = \Sigma_{n=1}^{N} \tau_{n-1}$ is the sum of the times of flight $\tau_n = \tau(\mathbf{z}_n)$ between N successive collisions, and $p_n^2/2m$ is the kinetic energy of a particle at the nth collision (see Appendix). The quantity $B_v^{(+)}(n)$ is related to the curvature of an expanding wave front of trajectories accompanying the particle and evaluated just after the nth collision. This quantity is given by recursion according to the following continuous fraction,

$$B_v^{(+)}(n) = \frac{2mg}{p_n \cos\varphi_n} \left(\frac{\kappa_n}{m^2 g} p_n^2 - \sin\alpha_n \right) + \frac{1 - \dfrac{m^2 g^2 \tau_{n-1}^2}{p_{n-1}^2}}{\tau_{n-1} \dfrac{p_{n-1}^2 + p_n^2 - m^2 g^2 \tau_{n-1}^2}{2 p_n^2} - \dfrac{1}{\dfrac{2 m^2 g^2 \tau_{n-1}}{p_{n-1}^2} - \left(1 - \dfrac{m^2 g^2 \tau_{n-1}^2}{p_{n-1}^2} \right) B_v^{(+)}(n-1)}}, \quad (5)$$

where κ_n is the curvature of the floor, α_n denotes the angle between the outer normal to the floor and the horizontal line, and φ_n is the angle between the normal and the outgoing velocity, all these quantities being evaluated at the nth collision point.

In the following, we consider that the floor is made of parabolic tiles

$$y = -\frac{1}{2r}(x-l)^2 \quad \text{for} \quad l - \frac{1}{2} < x < l + \frac{1}{2}, \quad (6)$$

where l is an integer. Moreover, the successive parabolas intersect with each other at right angle of 90°, as shown in Fig. 1. This condition imposes that $r = 1/2$. We choose $y = 0$ as the top of the parabola. Therefore, the particle is trapped in one of the intervals $|x - l - 1/2| \leqslant (1/2) - \sqrt{-2Er/mg}$ if its energy is negative, although the particle is no longer trapped if its energy is positive.

If the energy of the particle is negative and so small that the curvature in the vicinity of the intersection is almost negligible, its dynamics is completely chaotic because the system can then be very well approximated by a wedge billiard that is fully chaotic as proven in the case where the angle of the wedge is larger than 90° [11,12]. However, in this case, the particle is confined in a hole near the intersection of two successive parabolas. As energy increases, the curvature of the floor starts to play a very important role.

If the total energy is positive, the particle can jump over the parabolas and wander in an unbounded diffusive motion. An important threshold occurs at the critical energy $E_{\text{th}} = mgr/2$. At this threshold, the point particle launched from the intersection between two parabolas flies to the next intersection by creeping the parabolic floor.

In Eq. (6), it turns out that, if the energy is very small, the curvature contribution $(\kappa_n/m^2 g)p_n^2$ is less than the contribution $\sin\alpha_n$ due to the slope of the floor. Both contributions cancel out each other precisely at an energy equal to the threshold $E_{\text{th}} = mgr/2$, where the point particle launched from the intersection between two parabolas flies to the next intersection by creeping the parabolic floor. The curvature contribution becomes larger than the slope contribution above the threshold energy E_{th}. Indeed, the system has a nearly fully chaotic dynamics above this threshold due to the defocusing character of the collisions on the floor, and all the stability islands are much smaller than the size of the Birkhoff phase space as shown in Fig. 2.

In Fig. 6, we depict by a dotted line, the average value of the Lyapunov exponent of our system. We observe that, on

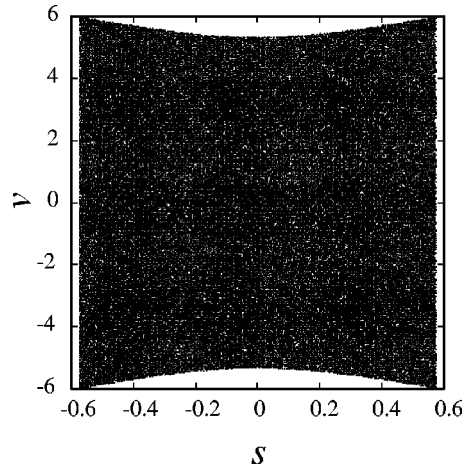

FIG. 2. Phase portraits of the billiard in the space of Birkhoff coordinates (s,v) corresponding to one parabolic tile at the energy $E = 14.2$. The chaotic sea covers most of phase space.

average, the Lyapunov exponent is positive, showing that our system is indeed chaotic. The observed dependence on energy can be understood by supposing that the instability is caused by the defocusing character of the collisions on the corrugations of the floor. Since the trajectory is parabolic between the collisions, we can estimate the perturbation on the horizontal position x_{n+1} at the $(n+1)$th collision that is caused by a perturbation on the angle θ_n between the velocity and the horizontal axis at the nth collision. At high energies, most of the jumps reach a height that is larger than the corrugations of the floor so that $x_{n+1} \simeq x_n + (v_n^2/g)\sin(2\theta_n)$ because the trajectory is a parabola. Accordingly, the perturbation on the next horizontal position is of the order of $\delta x_{n+1} \sim (E/mg)\,\delta\theta_n$. The perturbation on the next angle is $\delta\theta_{n+1} \sim \delta x_{n+1}/r$ because the radius of curvature of the floor is approximately equal to r. Hence, the perturbation on the angle is amplified according to $\delta\theta_{n+1} \sim (E/mgr)\,\delta\theta_n$ at each collision, so that the average Lyapunov exponent of the map is estimated as $\lambda_{\rm map} \sim \ln(\delta\theta_{n+1}/\delta\theta_n) \sim \ln(E/mgr)$. On the other hand, the average vertical and horizontal velocities scale like $\sqrt{\langle v_x^2\rangle} \sim \sqrt{\langle v_y^2\rangle} \sim \sqrt{E/m}$. Therefore, the average time of flight scales like $\langle\tau\rangle \sim \sqrt{\langle v_y^2\rangle}/g \sim \sqrt{E/mg^2}$. Since the average Lyapunov exponent of the flow is equal to the average Lyapunov exponent of the map divided by the average time of flight, $\lambda = \lambda_{\rm map}/\langle\tau\rangle$, we infer that the Lyapunov exponent decreases as $\lambda \sim (g\sqrt{m/E})\ln(E/mgr)$ in the limit $E \to \infty$ in agreement with the behavior observed in Fig. 6.

IV. PHASE DIAGRAM

We have also studied the local behavior of the Lyapunov exponent in order to investigate the nonhyperbolicity of our system. When the initial point is in an elliptic island, the local Lyapunov exponent of the orbit is vanishing. On the other hand, we observed that the local Lyapunov exponent of an orbit of the chaotic sea is positive and larger than one. Accordingly, the existence of elliptic islands can be numerically investigated with the local Lyapunov exponent.

Taking into consideration the symmetry of the phase space of the Birkhoff coordinate, we have taken 1 000 000 initial points distributed over a quarter of the phase space. Using the local Lyapunov exponents, we have been able to find very small elliptic islands that cannot be detected otherwise in a phase portrait. For example, the orbit in Fig. 2 is chaotic, and no elliptic island seems to exist in the phase portrait. However, the method of the local Lyapunov exponents detects the tiny elliptic islands shown in Fig. 3.

In the phase diagram of Fig. 4, each black square denotes a parameter value where at least one elliptic island is detected by the aforementioned method. One can recognize structures that are reminiscent of the Arnold tongues. The white regions of the phase diagram of Fig. 4 may correspond either to systems with undetected extremely small elliptic islands, or to fully chaotic systems.

In Fig. 4, one can see a periodic structure of energies, which can be understood as follows. As energy increases the maximum jump also increases. When the total energy E of the particle is in the range of $[(l-1/2)mg/2,(l+1/2)mg/2]$, the particle can jump over l tiles if it starts from an intersection between two parabolas. (We have here taken the value $r=1/2$.) Since the floor is periodic a similar behavior happens if the maximum jump reaches a similar point, which occurs at the energies $E_l=(l-1/2)mg/2$ with $l=1,2,3,\ldots$. Hence, similar structures appear repetitively over the period $\Delta E = mg/2$.

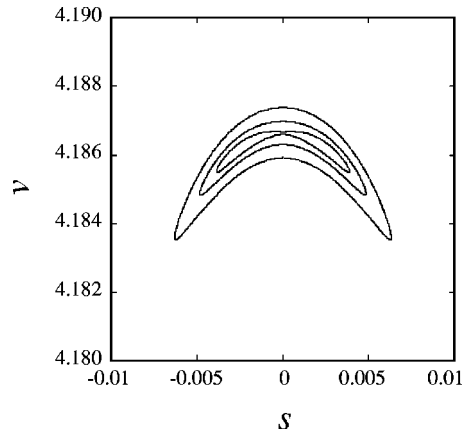

FIG. 3. Enlargement of the small region of the space of Birkhoff coordinates (s,v) where we observe the elliptic island at the same energy as in Fig. 2.

On the line of $r=0.5$, all the islands are much smaller than the whole energy surface at the energies above the threshold $E_{\rm th}$.

V. DIFFUSIVE TRANSPORT IN ABSENCE OF NOISE

The diffusion coefficient is defined by Einstein's formula,

$$D = \lim_{t\to\infty} \frac{1}{2t}\langle [x(t)-x(0)]^2\rangle, \tag{7}$$

where the average $\langle\cdot\rangle$ is carried out over a statistical ensemble of initial conditions that could be distributed uniformly in the Birkhoff phase space. The diffusion coefficient can be expressed by a Green-Kubo formula in terms of the iterative dynamics given by Eqs. (3) as

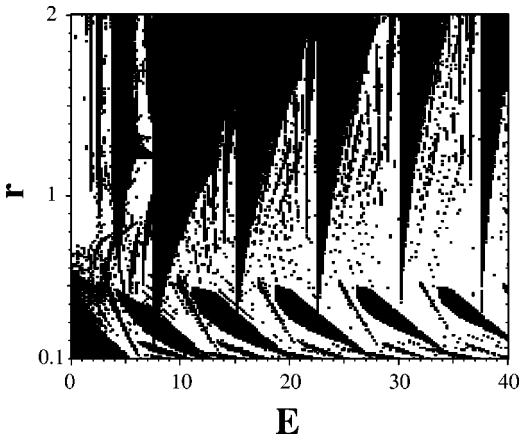

FIG. 4. Phase diagram in the case of the floor made of parabolic tiles. The black squares denote the existence of elliptic periodic orbits.

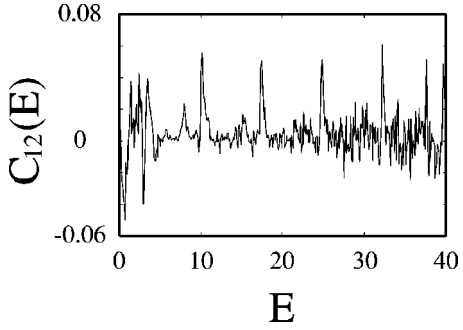

FIG. 5. The jump autocorrelation function at the 12th collision vs energy. The peaks appear at the energies where elliptic periodic orbits without horizontal particle transport exist.

$$D=\frac{1}{2\langle\tau\rangle}\sum_{n=-\infty}^{+\infty}\langle a(\mathbf{z})a(\mathbf{f}^n\mathbf{z})\rangle, \tag{8}$$

where the average $\langle\cdot\rangle$ is carried out over the uniform probability distribution in the Birkhoff phase space [13]. The Green-Kubo formula relates the autocorrelation function with the diffusion coefficient. We emphasize that Eq. (8) gives the diffusion coefficient of the continuous-time dynamics. The autocorrelation function is defined by

$$C_n(E)\equiv\langle a(\mathbf{z})a(\mathbf{f}^n\mathbf{z})\rangle, \tag{9}$$

where n is the number of collisions.

If this autocorrelation function would decay algebraically because of a sticking to an elliptic island, we cannot expect a finite diffusion coefficient. Such algebraic decays of the autocorrelation funcion occur in the presence of elliptic islands, which represents many parameter values as seen in the phase diagram of Fig. 4. Especially, the elliptic islands centered on a localized periodic orbit that do not transport particles in the horizontal direction strongly affect the autocorrelation function, as shown in Fig. 5. One can see that the autocorrelation function has peaks corresponding to values of the energy where the aforementioned periodic orbits exist. In such a case, we cannot expect that the diffusion coefficient is finite because the autocorrelation function does not decay to zero.

However, the phase diagram also shows the possibility that no elliptic island exists in certain energy ranges that are the blank region in Fig. 4. In the absence of elliptic island, we would expect that an effective diffusion coefficient exists and is finite. This diffusion coefficient has been calculated numerically and is depicted in Fig. 6 as a function of energy. In Fig. 6, we observe a rich structure depending on the energy scale. This structure is numerically reproducible and is not due to statistical fluctuations in the numerical calculation.

The curve of the diffusion coefficient has a very irregular fine structure. The inset of Fig. 6 depicts a zoom on the curve showing the persistence of fine structures on smaller energy scales. This apparent self-similar behavior has also been observed in a piecewise-linear one-dimensional mappings as the diffusion coefficient varies with the slope [6–9]. Here, a very analogous behavior is observed in a mechanical system as the energy of the particle is varied. This complex behavior

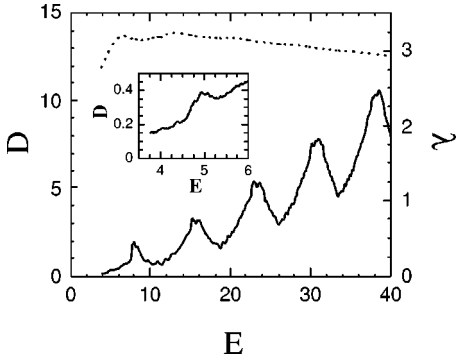

FIG. 6. Diffusion coefficient D (solid line) and Lyapunov exponent λ (dashed line) vs energy E (above the threshold energy $E_{\rm th}=mgr/2=mg/4=3.75$). The diffusion coefficient oscillates with the period $\Delta E=mg/2=7.5$. Inset: Zoom on the beginning of the curve of the diffusion coefficient, showing the irregularity of this curve on smaller scales.

has its origin in the fact that the topology of the trajectories changes with energy, i.e., the system is not structurally stable.

In order to understand in more detail this strange behavior we have considered the energy dependence of each of the autocorrelation coefficients $C_n(E)=\langle a(\mathbf{z})a(\mathbf{f}^n\mathbf{z})\rangle$ in the series of Eq. (8). Each one of these coefficients has a smooth dependence on energy but the sum of them turns out to be irregular. The autocorrelation coefficients $C_n(E)$ are numerically observed to decay exponentially with the number n of collisions, as seen in Fig. 7(a). Consequently, we would infer that the series (8) converges to a finite diffusion coefficient. On the other hand, the autocorrelation coefficients $C_n(E)$ oscillate with the energy E more and more rapidly as n increases because the sensitivity to initial conditions generates a sensitive dependence on the control parameter E. Indeed, in each derivative $(d/dE)C_n(E)$, we find products of the type $\Pi_{k=m+1}^{n-1}(\partial\mathbf{f}/\partial\mathbf{z})(\mathbf{f}^k\mathbf{z})\cdot(\partial\mathbf{f}/\partial E)(\mathbf{f}^m\mathbf{z})$ with $m=0,\ldots,n-2$. Such products grow exponentially in a way controlled by the Lyapunov exponents of the map $\mathbf{f}$. Accordingly, we can expect that the derivatives $dC_n(E)/dE$ do not decay with the n number of collisions. We have confirmed this expectation by a numerical evaluation of these derivatives that indeed do not decay as $n\to\infty$ [see Fig. 7(b)].

These properties are reminiscent of those of the Weierstrass function

$$W(E)=\sum_{n=0}^{\infty}\alpha^n\sin(\beta^nE), \tag{10}$$

which is known to be nowhere differentiable provided that $0<\alpha<1$, $\beta>1$, and $\alpha\beta\geqslant 1$ [15]. For the Weierstrass function, the terms decay exponentially in the series (10) although they grow in the series defining the derivative dW/dE. A very similar behavior is here observed for the diffusion coefficient of our system. Therefore, we think that the series $\Sigma_{n=1}^{\infty}dC_n(E)/dE$ do not converge so that the diffusion coefficient (8) is a nondifferentiable function of energy in analogy with the Weierstrass function.

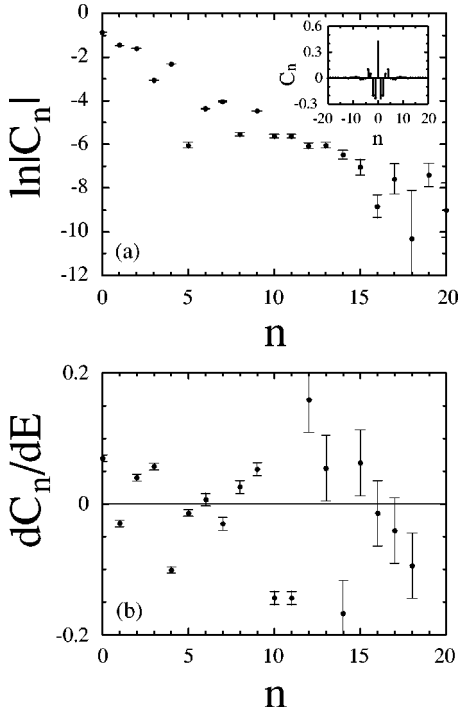

FIG. 7. (a) Decay of the autocorrelation coefficient $C_n(E)=\langle a(\mathbf{z})a(\mathbf{f}^n\mathbf{z})\rangle$ vs n, at the energy $E=5$. The main figure depicts $|C_n|$ vs n with a vertical logarithmic scale while the inset depicts C_n vs n in order to show its oscillations. (b) Derivatives $dC_n(E)/dE$ vs n at the same energy.

The result of this section clearly shows that the effective diffusion coefficient has an irregular dependence on the energy of the particle. This phenomenon is reminiscent of a similar behavior observed in piecewise-linear maps [6–9]. However, we should notice that these piecewise-linear maps are strictly hyperbolic, while the present system is not. Therefore, part of the irregularity could be attributed to the fact that the energy values at which elliptic islands exist form a set in the phase diagram that is like a dense set. In this case, the structural instability of the topology of trajectories would be more important compared to the case of expanding piecewise-linear maps with a varying slope.

VI. DIFFUSION IN THE PRESENCE OF NOISE

The small elliptic islands are easily destroyed by the perturbation of a weak noise. Indeed, we have introduced a weak noise in our system by changing at random the direction of the velocity just after an elastic collision. This noise is weak in the sense that the velocity angle is randomly perturbed by small angles less than $\pm\epsilon\pi/2$. Therefore, the energy of the particle does not change. With such noises, the iterative dynamics is modified as

$$\mathbf{z}_{n+1}=\mathbf{F}(\mathbf{z}_n;\eta_n),$$
$$v_{n+1}=\cos\eta_n v'_{n+1}+\sin\eta_n\sqrt{2E/m-2gy_{n+1}-v'^2_{n+1}}, \tag{11}$$
$$(x_{n+1},v'_{n+1})=\mathbf{f}(\mathbf{z}_n).$$

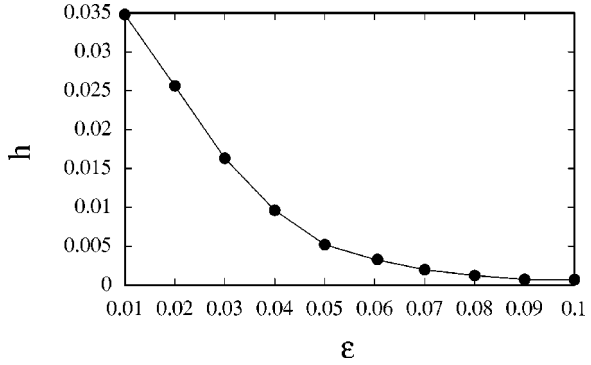

FIG. 8. The heights of the peaks of the autocorrelation function around the energy equal to 10, as a function of the noise amplitude ϵ. The peaks decrease as the intensity ϵ of noise increases.

In Eq. (11), η_n is a random number uniformly distributed in $[-\epsilon_1,\epsilon_2]$, where

$$\epsilon_1=\min\left\{\frac{\pi}{2}\epsilon,\alpha\right\} \tag{12}$$

and

$$\epsilon_2=\min\left\{\frac{\pi}{2}\epsilon,\pi-\alpha\right\}, \tag{13}$$

α being the angle between the postcollision velocity and the unit vector tangent to the floor at the point of collision.

This weak noise has the effect that the peaks of the autocorrelation function due to the elliptic islands decrease as the intensity of the noise increases. These peaks almost vanish at noise intensities ϵ larger than 0.08, as shown in Fig. 8.

We also notice that the peaks of the autocorrelation functions decrease faster at the energy around 14 than that at the energy around 10 as shown in Fig. 9. Therefore, we conclude that the higher the energy of a particle, the faster the peaks of autocorrelation function decrease.

Figure 10 depicts the autocorrelation function of the system perturbed by a weak noise at the intensity ϵ equal to

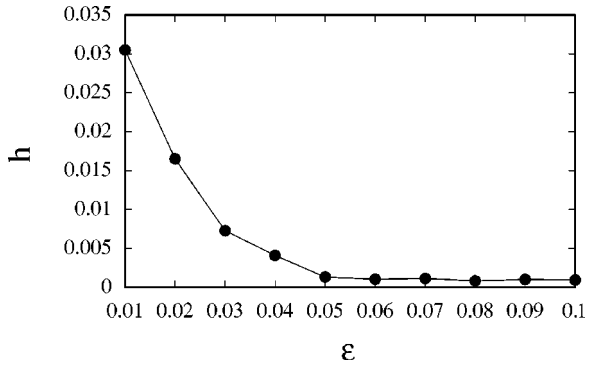

FIG. 9. The heights of the peaks of the autocorrelation function around the energy equal to 14, as a function of the noise amplitude ϵ. We observe that the heights decreases faster than for an energy equal to 10.

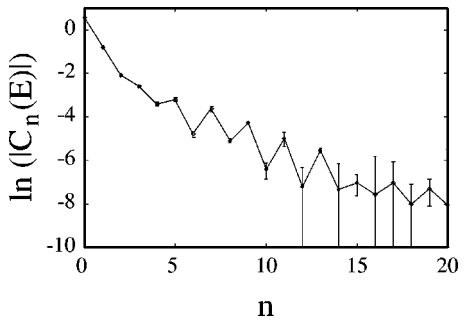

FIG. 10. The autocorrelation function with small noises of amplitude $\epsilon=0.08$ at the energy $E=10$. The autocorrelation decays very fast like an exponential as the collision time n increases.

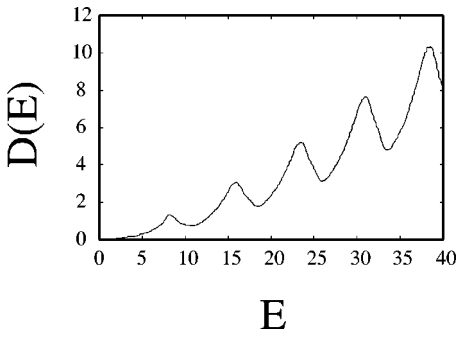

FIG. 11. Diffusion coefficient D vs energy E in the presence of a weak noise. We observe that the diffusion coefficient oscillates with the period $\Delta E=mg/2=7.5$.

0.08. One can see that the autocorrelation function rapidly decays in an exponential-like behavior, in the presence of a weak noise.

Since the size of the elliptic islands is always much smaller than the size of the phase space in the present system, the orbits can escape from the elliptic islands under the effect of a weak noise. Indeed, we have observed that the autocorrelation function decays exponentially already for weak noises. Accordingly, normal diffusion and a finite diffusion coefficient can be expected already for such weak noise.

When the system is perturbed by small noises, the diffusion coefficient is also given by Eq. (7) but where the average $\langle\cdot\rangle$ is now carried out over both a uniform probability distribution in the Birkhoff phase space and over the noise. This diffusion coefficient has been calculated numerically and is depicted in Fig. 11 as a function of energy. The dependence on energy is very similar to the one in the absence of noise seen in Fig. 6. However, the fine irregular structures are now smoothened as expected. Nevertheless, there remains an oscillatory dependence on energy superimposed on an increase of the diffusion coefficient with energy.

This gross increase of the diffusion coefficient with energy can be explained by considering a random-walk model as in Ref. [16]. In such a random walk, the mean free flight can be estimated as the mean intercollision time multiplied by the average horizontal velocity of the particle: $L\sim\sqrt{\langle v_x^2\rangle}\langle\tau\rangle$. Since the diffusion coefficient is roughly equal to the square of the mean free flight divided by the intercollisional time, we infer that $D\sim L^2/\langle\tau\rangle\sim g^{-1}(E/m)^{3/2}$, which explains the gross increase of the diffusion coefficient with energy.

Besides, the oscillations of the diffusion coefficient with energy can be understood in the same way of the periodic structure seen in the phase diagram of Fig. 4. Accordingly, the diffusion coefficient oscillates with energy with the period $\Delta E=mg/2$.

VII. ESTIMATION OF THE DIFFUSION IN THE CASE OF INFINITE RADIUS OF THE CURVATURE

When the radius of curvature of the floor is infinitely large, we will show that there exists an invariant subset of trajectories, which has a fully chaotic dynamics. The method we use is inspired by the work of Hénon [17].

A. Derivation of a piecewise-linear mapping

The horizontal position x_1 and the velocity v_1 tangent to the floor after one flight between collisions are obtained by solving the Hamilton equation. Hence, one can express them explicitly by the initial horizontal position x_0 and the initial horizontal and vertical velocities, u_{x0} and u_{y0},

$$x_1=x_0+\left(\frac{g}{u_{x0}^2}-\frac{1}{r}\right)^{-1}\left[\left(\frac{x_0}{r}+\frac{u_{y0}}{u_{x0}}-\frac{c_1}{r}\right)\pm\sqrt{\left(\frac{x_0}{r}+\frac{u_{y0}}{u_{x0}}-\frac{c_1}{r}\right)^2+\frac{2(c_0-c_1)}{u_{x0}^2 r}\left\{u_{x0}u_{y0}+g\left(x_0-\frac{c_0+c_1}{2}\right)\right\}}\right], \quad (14)$$

and

$$v=\left\{1+\frac{1}{r^2}(x_1-c_1)^2\right\}^{-1/2}\left\{u_{x0}-\frac{1}{r}(x_1-c_1)\left(u_{y0}-g\frac{x_1-x_0}{u_{x0}}\right)\right\}. \quad (15)$$

Here c_0 and c_1 denote the integers equal to the centers of the tiles where the particle starts and arrives, respectively.

We assume that the radius of the curvature at the top of the tile is infinitely large, and the particle starts in almost vertical directions. Therefore, we can neglect the terms of the order of r^{-1} and obtain

$$x_1 = x_0 + \frac{2u_{x0}u_{y0}}{g}, \tag{16}$$

and

$$v_1 = u_{x0} + \frac{u_{y0}}{r}(x_1 - c_1). \tag{17}$$

By the same approximation, we have

$$v_0 = u_{x0} - \frac{u_{y0}}{r}(x_0 - c_0). \tag{18}$$

Substituting Eq. (18) into Eq. (16) yields

$$x_1 = x_0 + \frac{2u_{y0}^2}{gr}(x_0 - c_0) + \frac{u_{y0}}{r}v_0. \tag{19}$$

From Eqs. (17) and (18), we get

$$v_1 = v_0 + \frac{u_{y0}}{r}\{(x_0 - c_0) + (x_1 - c_1)\}. \tag{20}$$

We have assumed that the horizontal velocity and the height of the tile is extremely small so that we obtain

$$u_{y0} = \sqrt{\frac{2E}{m}}. \tag{21}$$

From Eqs. (19), (20), and (21), we get

$$x_1 = x_0 + \frac{4E}{mgr}(x_0 - c_0) + \frac{2}{g}\sqrt{\frac{2E}{m}}v_0, \tag{22}$$

and

$$v_1 = v_0 + \frac{1}{r}\sqrt{\frac{2E}{m}}\{(x_0 - c_0) + (x_1 - c_1)\}. \tag{23}$$

Note that this mapping is area preserving because the assumption of the infinite radius of curvature makes the horizontal momentum conjugate to the horizontal position.

Following Hénon and for simplicity [17], we change the scale of the velocity v to w,

$$w \equiv \left\{ \sqrt{\frac{g}{2r}\left(2 + \frac{4E}{mgr}\right)} \right\}^{-1} v, \tag{24}$$

and define a new parameter ϕ,

$$\phi \equiv \cosh^{-1}\left(1 + \frac{4E}{mgr}\right). \tag{25}$$

Thus, we finally obtain the following symplectic mapping:

$$x_{j+1} = (x_j - c_j)\cosh\phi + w_j \sinh\phi + c_j \tag{26}$$

and

$$w_{j+1} = (x_j - c_j)\sinh\phi + w_j \cosh\phi + (c_j - c_{j+1})\tanh\frac{\phi}{2}, \tag{27}$$

where j denotes the number of collisions. Note that the dimension of w is the same as x.

B. Construction of a chaotic subset

We show that there exist orbits for which the horizontal momentum always remains small during the whole time evolution.

Substituting x_j and w_j by recursion, one can obtain

$$\begin{aligned} x_j - c_j = {} & (x_0 - c_0)\cosh j\phi + w_0 \sinh j\phi \\ & + \sum_{k=1}^{j} \frac{1}{\sinh\phi}(c_{k-1} - c_k)\{\sinh(j-k+1)\phi \\ & - \sinh(j-k)\phi\}, \end{aligned} \tag{28}$$

and

$$\begin{aligned} w_j = {} & (x_0 - c_0)\sinh j\phi + w_0 \cosh j\phi + \sum_{k=1}^{j} \frac{1}{\sinh\phi}(c_{k-1} - c_k) \\ & \times\{\cosh(j-k+1)\phi - \cosh(j-k)\phi\}. \end{aligned} \tag{29}$$

Accordingly, the sum of the above terms yields

$$\begin{aligned} (x_j - c_j + w_j)e^{-j\phi} = {} & x_0 - c_0 + w_0 + \frac{2e^{\phi}}{e^{\phi}+1} \\ & \times \sum_{k=1}^{j} (c_{k-1} - c_k)e^{-k\phi}. \end{aligned} \tag{30}$$

The horizontal distance and the velocity of one flight has a maximum because the energy E is finite. Therefore, the term $(x_j - c_j + w_j)$ does not increase exponentially as the number of collision times increases without bound. Hence the left-hand side of Eq. (30) should vanish as j goes to infinity, and we obtain

$$x_0 + w_0 = \frac{e^{\phi}-1}{e^{\phi}+1}\left(c_0 + 2\sum_{k=1}^{\infty} c_k e^{-k\phi}\right). \tag{31}$$

In the same way, we also obtain

$$x_0 - w_0 = \frac{e^{\phi}-1}{e^{\phi}+1}\left(c_0 + 2\sum_{k=-\infty}^{-1} c_k e^{-k\phi}\right). \tag{32}$$

From Eqs. (31) and (32), the initial position and momentum are expressed by the integers corresponding to the centers of the tiles,

$$x_0=\frac{e^{\phi}-1}{e^{\phi}+1}\left\{c_0+\sum_{k=1}^{\infty}(c_k+c_{-k})e^{-k\phi}\right\}, \tag{33}$$

and

$$w_0=\frac{e^{\phi}-1}{e^{\phi}+1}\left\{\sum_{k=1}^{\infty}(c_k-c_{-k})e^{-k\phi}\right\}. \tag{34}$$

Therefore, we also have

$$x_j=\frac{e^{\phi}-1}{e^{\phi}+1}\left\{c_j+\sum_{k=1}^{\infty}(c_{j+k}+c_{j-k})e^{-k\phi}\right\}, \tag{35}$$

and

$$w_j=\frac{e^{\phi}-1}{e^{\phi}+1}\left\{\sum_{k=1}^{\infty}(c_{j+k}-c_{j-k})e^{-k\phi}\right\}. \tag{36}$$

We derived the piecewise-linear mapping (26) and (27) by assuming that the particle always bounces almost vertically, and hence the piecewise-linear mapping does not describe the orbits for which the momentum becomes large during the time evolution. Accordingly, we focus on those orbits that jump l tiles at most. Thus, we obtain an invariant subset that is infinitely extended in position, but finite in momentum. The dynamics on this invariant subset is always hyperbolic because the Lyapunov exponent of the map is equal to ϕ. This invariant subset is thus composed of unstable orbits.

From Eq. (27), the previous assumption yields

$$-\left(\frac{1}{2}+l\right)\leqslant(x_j-c_j)\cosh\phi+w_j\sinh\phi\leqslant\left(\frac{1}{2}+l\right), \tag{37}$$

which leads to

$$e^{\phi}\geqslant\sqrt{1+4l}. \tag{38}$$

The horizontal position x_j should always exist in the tile of the number c_j,

$$-\frac{1}{2}<x_j-c_j<\frac{1}{2}. \tag{39}$$

On the other hand, from Eq. (35), we have

$$x_j-c_j=\frac{e^{\phi}-1}{e^{\phi}+1}\left[\sum_{k=1}^{\infty}\{(c_{j+k}-c_j)+(c_{j-k}-c_j)\}e^{-k\phi}\right]. \tag{40}$$

Since the maximum jump is l, we obtain from Eq. (40) that

$$-\frac{e^{\phi}-1}{e^{\phi}+1}\left\{2l\sum_{k=1}^{\infty}ke^{-k\phi}\right\}\leqslant x_j-c_j\leqslant\frac{e^{\phi}-1}{e^{\phi}+1}\left\{2l\sum_{k=1}^{\infty}ke^{-k\phi}\right\}. \tag{41}$$

From Eqs. (39) and (41), we finally obtain

$$e^{\phi}>2l+\sqrt{4l^2+1}. \tag{42}$$

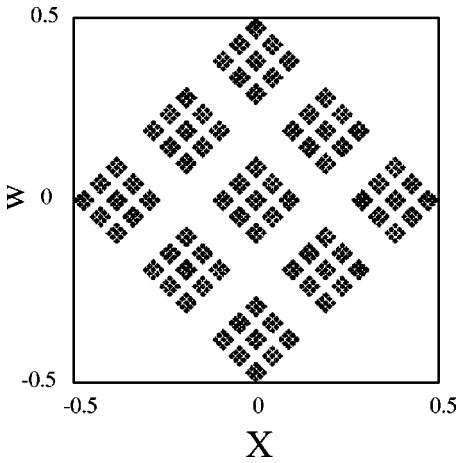

FIG. 12. The chaotic invariant subset in the case where the floor has an infinitely small curvature. In this case, $E=15\sqrt{(5-1)}/2, m=1, g=15, r=2$. The maximum jump l is equal to 1.

Note that the condition (42) automatically contains the condition (38).

If the energy of the particle satisfies Eq. (42), the dynamics on the invariant subset can be described by a symbolic dynamics made of the infinite symbols $\{\ldots,-2,-1,0,1,2,\ldots\}$. An example of the invariant subset considered in this section is depicted in Fig. 12.

C. Estimation of the diffusion coefficient

The mean square of the displacement of a flight over the invariant subset grows linearly to the increase of time. Accordingly, we can obtain an estimation of the diffusion coefficient of the system based on the dynamics restricted to this invariant subset.

The diffusion coefficient D can be evaluated by a statistical average over the invariant subset. Using Eq. (35), one can obtain

$$\langle(x_t-x_0)^2\rangle=\frac{1}{3}l(l+1)\left\{t+\frac{2}{(e^{\phi}+1)^2}te^{-(t-1)\phi}+\frac{4(e^{2\phi}+e^{\phi}+1)}{(e^{\phi}-1)(e^{\phi}+1)^3}e^{\phi}(e^{-t}-1)\right\}, \tag{43}$$

so that an approximate value of the diffusion coefficient is given by

$$D=\frac{1}{6}l(l+1). \tag{44}$$

It is important that the time τ of one flight is constant because we assumed that the orbit of the particle is almost always vertical, and hence we have

$$\tau=\frac{2}{g}\sqrt{\frac{2E}{m}}. \tag{45}$$

The minimum energy for the complete symbolic dynamics with maximum jump l is given by replacing the inequality of Eq. (42) to an equality,

$$2l+\sqrt{4l^2+1}=1+\frac{4}{mgr}E+\sqrt{\frac{4}{mgr}E\left(2+\frac{4}{mgr}E\right)}, \tag{46}$$

and thus we obtain

$$l=\sqrt{\frac{2E}{mgr}\left(1+\frac{2E}{mgr}\right)}. \tag{47}$$

Therefore, from Eqs. (44), (45), and (47), we can estimate the energy dependence of diffusion coefficients from below as the energy becomes large,

$$D\sim\frac{1}{3\sqrt{2}gr^2}\left(\frac{E}{m}\right)^{3/2}. \tag{48}$$

Note that this estimation is consistent with our previous result derived by the consideration of a random walk in the last section.

In the same way, one can obtain the velocity autocorrelation function

$$C(t)\equiv\langle(x_{t+1}-x_t)(x_1-x_0)\rangle = \frac{1}{3}l(l+1)\left(\frac{e^{\phi}-1}{e^{\phi}+1}\right)^2\left(|t|+\frac{e^{2\phi}+1}{e^{2\phi}-1}\right)e^{-|t|\phi}, \tag{49}$$

which allows us to confirm the value (44) of the diffusion coefficient by using the Green-Kubo formula,

$$D=\frac{C(0)}{2}+\sum_{t=1}^{\infty}C(t). \tag{50}$$

D. Lower bound on the topological entropy

Thanks to the invariant subset, we can also obtain a lower bound on the topological pressure function [13,18] as

$$P(\beta)\geqslant\ln(2l+1)-\beta\phi. \tag{51}$$

The pressure function is known to give the topological entropy at $\beta=0$. Accordingly, we obtain a lower bound on the topological entropy of the system as

$$h_{\mathrm{top}}=P(0)\geqslant\ln(2l+1). \tag{52}$$

Moreover, we can obtain the value of the Hausdorff dimension of the invariant subset of orbits considered in this section. Indeed, the partial Hausdorff dimension in the stable or unstable directions is known to be given by the zero of the pressure function as $P(d_{\mathrm{H}})=0$, so that we get

$$D_{\mathrm{H}}=2d_{\mathrm{H}}=2\frac{\ln(2l+1)}{\phi}. \tag{53}$$

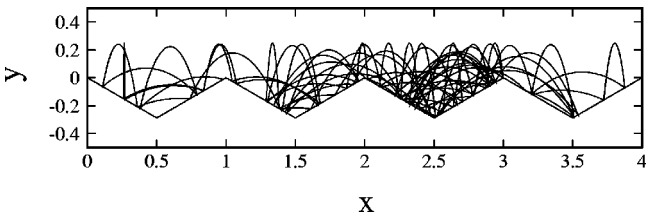

FIG. 13. The spatially extended billiard composed of a point particle moving in a downward vertical field and bouncing on a sawtooth-shaped floor. The angle of the edge is $2\pi/3$. In our case, $m=1$ and $g=15$.

Note that the Hausdorff dimension is less than 2 because of Eq. (42).

In this section, we have studied the dynamics of our chaotic billiard in an external field in the limit where the curvature of the floor is arbitrarily small. By deriving a piecewise-linear mapping, we have shown that there exists a hyperbolic invariant subset of orbits for which the particle always bounces almost vertically during its time evolution.

VIII. SAWTOOTH FLOOR

It is important to investigate other shapes of the floor in order to clarify the parameter dependence of the diffusion coefficient. In this section, we consider a floor made of triangle tiles,

$$y=-\frac{1}{2R}|x-l| \quad \text{for } l-\frac{1}{2}<x<l+\frac{1}{2}, \tag{54}$$

where l is an integer. Moreover, the successive triangles intersect with each other at the angle of 120°, as shown in Fig. 13.

This condition imposes that $R=\sqrt{3}/2$. We choose $y=0$ as the top of the triangle. Therefore, the particle is trapped in one of the intervals $|x-l-1/2|\leqslant(1/2+2ER/mg)$ if its energy is negative, although the particle is no longer trapped if its energy is positive.

When the energy of the particle is negative, its dynamics is completely chaotic because the system is precisely the same as a wedge billiard that is fully chaotic as proven in the case where the angle of the wedge is larger than 90° [11,12]. The Lyapunov exponent of the wedge billiards takes its maximum value when the angle of the intersection of the flat walls is 120° [11]. However, in these cases, the particle is confined in a hole near the intersection of two successive triangles.

If the total energy is positive, the particle can jump over the triangles and wander in an unbounded diffusive motion. Even for positive energies, elliptic periodic orbits and quasi-periodic orbits cannot be detected on a typical phase portrait. However, very small elliptic islands are detected by the methods of the local Lyapunov exponents explained in Sec. III, as shown in the phase diagram of Fig. 14. One can see the same periodic structure of the phase diagram with the period $\Delta E=mg/2$ as in the case of the floor made of parabolic tiles.

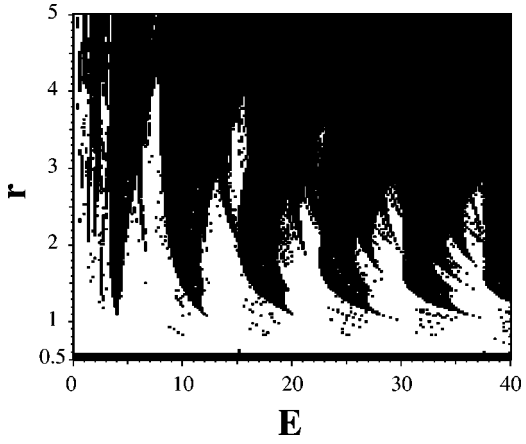

FIG. 14. Phase diagram in the case of the sawtooth floor. The black squares denote the existence of elliptic periodic orbits. We have that $r=2/\sqrt{3}R$.

The effective diffusion coefficient without noise is depicted in Fig. 15. The diffusion can be expected to be normal in those ranges of energies without elliptic island, i.e., where the black squares do not appear in Fig. 14. The diffusion coefficients do not oscillate in a well-pronounced periodic manner as in the case of the parabolic tiles.

For the sawtooth floor, the effective diffusion coefficient also shows a fine irregular structure as shown in the inset of Fig. 15. We have here also computed the jump autocorrelation function and its derivative with respect to energy, as shown in Fig. 16. One observe that the autocorrelation function decays very fast although its derivative does not appear to decay. Therefore, we expect a similar irregular dependence of the diffusion coefficient on energy as in the case of the floor made of parabolic tiles.

Moreover, we have also studied the average Lyapunov exponent in the case of the sawtooth floor. Since the curvature of the floor is zero, the collisions are not defocusing contrary to the case of parabolic tiles and we infer that the average Lyapunov exponent of the map does not depend on energy. On the other hand, the average vertical and horizontal velocities scale like $\sqrt{\langle v_x^2\rangle}\sim\sqrt{\langle v_y^2\rangle}\sim\sqrt{E/m}$. Therefore, the average time of flight scales like $\langle\tau\rangle\sim\sqrt{\langle v_y^2\rangle}/g\sim\sqrt{E/mg^2}$. The average Lyapunov exponent of the flow is equal to the average Lyapunov exponent of the map divided by the average time of flight, $\lambda=\lambda_{\mathrm{map}}/\langle\tau\rangle$. Hence, we infer that the Lyapunov exponent decreases as $\lambda\sim(g\sqrt{m/E})$ in the limit $E\to\infty$ in agreement with the behavior observed in Fig. 17.

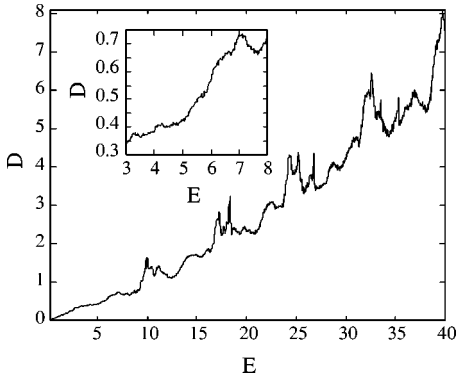

FIG. 15. Diffusion coefficient D vs energy E for the case of the sawtooth floor. The diffusion coefficient oscillates with the period $\Delta E=mg/2=7.5$. Inset: Zoom on the beginning of the curve of the diffusion coefficient, showing the irregularity of this curve on smaller scales.

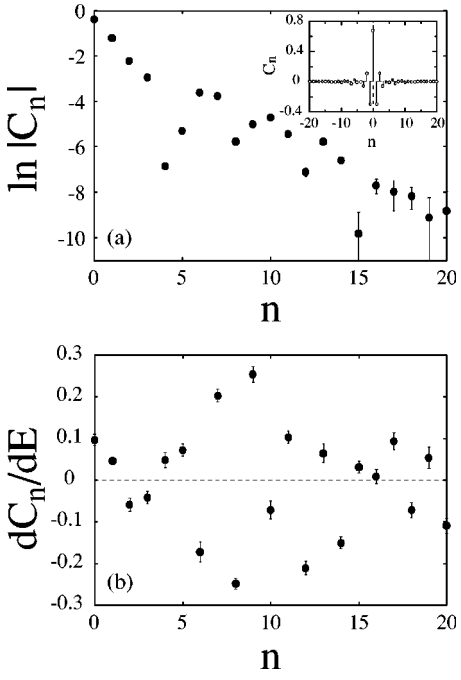

FIG. 16. (a) Decay of the autocorrelation coefficient $C_n(E)=\langle a(\mathbf{z})a(\mathbf{f}^n\mathbf{z})\rangle$ vs n, at the energy $E=3$. The main figure depicts $|C_n|$ vs n with a vertical logarithmic scale while the inset depicts C_n vs n in order to show its oscillations. (b) Derivatives $dC_n(E)/dE$ vs n at the same energy.

Therefore, the local Lyapunov exponents of the parabolic floor is much larger than that of the sawtooth floor. Both systems are chaotic and the islands are very small when they exist. However, the instabilities are very different as measured by the local Lyapunov exponents.

IX. SUMMARY AND CONCLUSION

In this paper, we have studied a class of chaotic billiards consisting of a point particle moving in a constant vertical

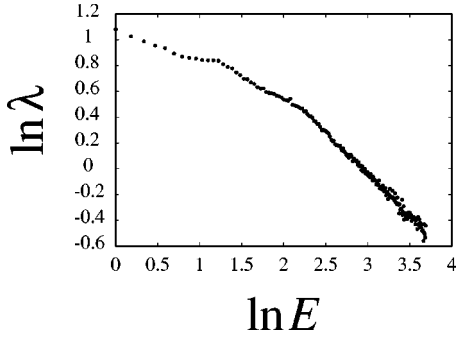

FIG. 17. Local Lyapunov exponent λ vs energy E in the case of the sawtooth floor.

field and bouncing on a periodically corrugated floor. Two kinds of floors have been investigated: one made of parabolic tiles and the other of triangular tiles.

In the case of parabolic tiles, we have shown that the dynamics is chaotic but nonhyperbolic and that this chaos induces a horizontal diffusive transport of the particle. This diffusion is normal if the deterministic motion is perturbed by a weak noise and the diffusion coefficient has an oscillatory dependence on energy. The present result clearly shows that an oscillatory dependence of a transport coefficient on the control parameters of a system is a common phenomenon that should be expected not only in abstract mappings like the standard mapping but also in mechanical systems such as the present billiards.

In the absence of noise, the nonhyperbolicity of the dynamics generates a very rich structure, both in phase space, in parameter space, as well as in the transport properties. We have here constructed by a method based on the local Lyapunov exponent a phase diagram in the parameter space of our system showing the regions where elliptic islands should be expected in the phase space. These regions have a complex structure reflecting the characteristic properties of the dynamics. The presence of the elliptic islands imply that the time autocorrelation function of the jump from tile to tile does not decay to zero so that the diffusion is not normal for such systems. However, in the apparent absence of elliptic island, the autocorrelation function is numerically observed to decay very fast, which suggests the existence of an effective diffusion coefficient. This effective diffusion coefficient has an irregular—but numerically reproducible—dependence on energy.

We have estimated analytically the diffusion in the case of the infinitely small curvature of the billiard wall and on the basis of an invariant subset of orbits in correspondence with a symbolic dynamics defined on an infinite alphabet of symbols. We have characterized this chaotic invariant subset in terms of its topological entropy and Hausdorff dimension.

In the case of the sawtooth floor, we have shown similar but different properties. We attribute the differences to the fact that the collisions on the walls of the triangular tiles are not defocusing contrary to the collisions on parabolic tiles. The phase diagram of the sawtooth floor shows the same structures as in the case of the parabolic-tiled floor. However, the diffusion coefficient of the sawtooth floor does not oscillate in the same well-pronounced manner as the parabolic-tiled floor. On the other hand, the effective diffusion coefficients has an irregular dependence on energy in both cases.

In the case that the particle is electrically charged and that its vertical acceleration is caused by an electric field, the diffusion coefficient would be proportional to the electric conductance. In this case, our billiard can find an experimental realization in the form of semiconducting devices. In semiconducting devices, the thermal fluctuations as well as the impurities introduce some noise that modifies the deterministic motion. Accordingly, the fine dependence of the diffusion coefficient on energy cannot be expected in such experiments.

On the other hand, the present work shows that the oscillatory dependence of the diffusion coefficient on energy is preserved by weak noises. This result suggests that such an oscillatory dependence may manifest itself in the electric conductance of such a semiconducting device.

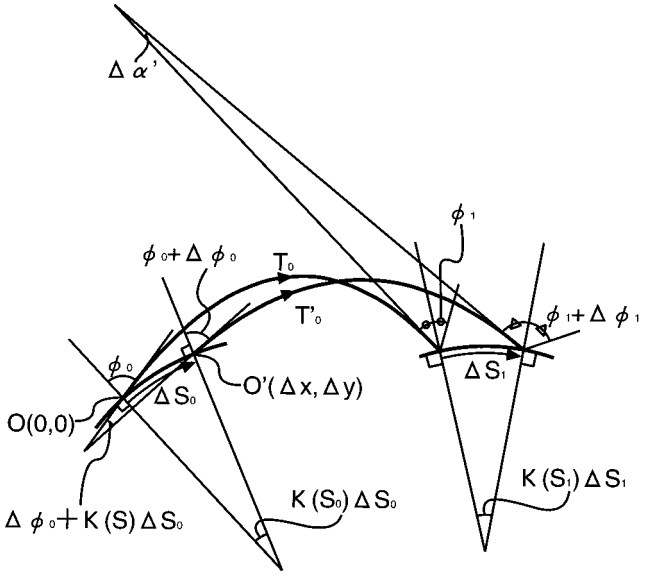

FIG. 18. The infinitesimal change of the original orbit at the collision point causes the infinitesimal change at the following collision.

ACKNOWLEDGMENTS

The authors thank Professor G. Nicolis and Dr. B. Komiyama for support and encouragement in this research, as well as Dr. R. Klages for fruitful discussions. T. H. is grateful to the Center for Nonlinear Phenomena and Complex Systems for hospitality. P. G. thanks the National Fund for Scientific Research (F.N.R.S. Belgium) for financial support, as well as the IAP Program of the Belgian Federal OSTC.

APPENDIX: LINEAR STABILITY OF BOUNCING PARTICLES

Let us suppose that a particle of mass m moves subject to a constant vertical acceleration g and launches from the floor at the origin $\mathbf{O}(0,0)$ with the angle φ_0 measured by the outer normal of the floor as shown in Fig. 18. The horizontal and vertical velocity of the particle at the origin are u_0 and v_0, respectively. Then the orbit $\mathbf{T_0}$ of the particle is

$$y=-\frac{g}{2u_0^2}x^2+\frac{v_0}{u_0}x. \tag{A1}$$

We consider another orbit $\mathbf{T}_0'$ of the particle of the same energy launching from the floor at the point $\mathbf{O}'$ $(\Delta x_0,\Delta y_0)$ infinitesimally close to the origin with the angle $\varphi+\Delta\varphi$. The horizontal and vertical velocity of this particle at the point $\mathbf{O}'$ are u_0' and v_0', respectively. Then we have

$$\Delta x_0=\sin(\gamma_0+\varphi_0)\Delta s_0,$$

$$\Delta y_0=-\cos(\gamma_0+\varphi_0)\Delta s_0, \tag{A2}$$

where

$$\frac{v_0}{u_0}=\tan\gamma_0, \tag{A3}$$

and Δs_0 is the distance between the points **O** and **O′**. Due to the conservation of the energy, we obtain

$$\frac{1}{2}mu_0^2+\frac{1}{2}mv_0^2=\frac{1}{2}mu_0^2+\frac{1}{2}mv_0^2+mg\Delta y. \tag{A4}$$

Neglecting the higher order terms of infinitesimal quantities yields

$$u_0\Delta u_0+v_0\Delta v_0=g\cos(\gamma_0+\varphi_0)\Delta s_0. \tag{A5}$$

The slope of the orbit $\mathbf{T}_0'$ at the point **O′** is

$$\frac{v_0'}{u_0'}=\tan[\gamma_0-\Delta\varphi_0-\kappa(s_0)\Delta s_0], \tag{A6}$$

where $\kappa(s_0)$ is the curvature of the floor at the origin **O** measured by the outer normal. In the case of the parabolic tiles described by Eq. (6) in the text, the curvature is given explicitly as

$$\kappa(s)=\frac{1}{r}\left\{1+\frac{1}{r^2}(x-l)\right\}^{-3/2}, \tag{A7}$$

where we supposed the x coordinate of the collision point s on the floor is contained in the region $(l-1/2,l+1/2)$.

From the leading order of the infinitesimal quantities of Eq. (A4), we obtain

$$u_0\Delta v_0-v_0\Delta u_0=(u_0^2+v_0^2)[-\Delta\varphi-\kappa(s_0)\Delta s_0]. \tag{A8}$$

From Eqs. (A5) and (A8), we obtain

$$\begin{pmatrix}\Delta u_0\\ \Delta v_0\end{pmatrix}=\begin{pmatrix}\dfrac{m^2g}{p_0^2}\cos(\gamma_0+\varphi_0)+v_0\kappa(s_0) & v_0\\ \dfrac{m^2g}{p_0^2}\cos(\gamma_0+\varphi_0)-u_0\kappa(s_0) & -u_0\end{pmatrix}\begin{pmatrix}\Delta s_0\\ \Delta\varphi_0\end{pmatrix}. \tag{A9}$$

By neglecting the second order of Δx, the orbit $\mathbf{T}_0'$ can be written as

$$y'=-\frac{g}{2u_0'^2}x'^2+\left(\frac{v_0'}{u_0'}+\frac{g}{u_0'^2}\Delta x_0\right)x'-\frac{v_0'}{u_0'}\Delta x_0+\Delta y_0. \tag{A10}$$

The floor can be approximated by the straight line in the vicinity of the point $\mathbf{C}(x,y)$ of the collision,

$$y'=\xi_1(x'-x)+y, \tag{A11}$$

where ξ_1 is the derivative of the curve of the floor. This approximation is enough for the evaluation of the shift Δs_1 that is the distance between the intersections of the orbits $\mathbf{T}_0$ and $\mathbf{T}_0'$ with the floor.

From Eqs. (A10) and (A11), we obtain

$$x_1=x_1+\frac{x_1}{\xi_1-A_1}\frac{1}{u_0}\left(-A_1\Delta u_0+\Delta v_0+\frac{g}{2u_0}\Delta x\right)+\frac{1}{\xi_1-A_1}\left(-\frac{v_0'}{u_0'}\Delta x_0+\Delta y_0\right), \tag{A12}$$

and hence

$$\Delta s_1=\frac{\sqrt{1+\xi_1^2}}{\xi_1-A_1}\frac{1}{u_0}\left(-A_1\Delta u_0+\Delta v_0+\frac{g}{2u_0}\Delta x\right)+\frac{\sqrt{1+\xi_1^2}}{\xi_1-A_1}\left(-\frac{v_0}{u_0}\Delta x_0+\Delta y_0\right), \tag{A13}$$

where A_1 is the derivative of the orbit $\mathbf{T}_0$ at the point (x,y),

$$A_1=-\frac{g}{2u_0^2}x+\frac{v_0}{u_0}. \tag{A14}$$

The infinitesimal difference $\Delta\varphi_1$ between the angles of the reflections of the orbits $\mathbf{T_0}$ and $\mathbf{T_0'}$ at the points (x,y) and (x',y') is

$$\Delta\varphi_1=\Delta\alpha'+\kappa(s_1)\Delta s_1, \tag{A15}$$

where $\Delta\alpha'$ is the infinitesimal angle between the lines tangent to the orbits $\mathbf{T}_0$ and $\mathbf{T}_0'$ as shown in Fig. 18. The derivative A_1' of the orbit $\mathbf{T}_0'$ at the point (x',y') is given in the first order of the infinitesimal angle $\Delta\alpha'$ as

$$A_1'=A_1+(1+A_1^2)\Delta\alpha'. \tag{A16}$$

From Eqs. (A12), (A15), and (A16), we obtain

$$\Delta\varphi_1=\frac{1}{1+A_1^2}\frac{1}{u_0}\left\{\left(-2A_1+\frac{v_0}{u_0}\right)\Delta u_0+\Delta v_0\right\}+\frac{1}{1+A_1^2}\frac{g}{u_0^2}(\Delta x_0-\Delta x_1)+\kappa(s_1)\Delta s_1. \tag{A17}$$

By substituting Eqs. (A2) and (A9) into Eqs. (A13) and (A17), we obtain

$$\begin{pmatrix} \Delta s_1 \\ \Delta \varphi_1 \end{pmatrix} = \begin{pmatrix} \dfrac{2\sqrt{1+\xi_1^2}}{\xi_1 - A_1}\left[-\dfrac{x_1}{u_0}A_1 - \dfrac{u_0}{g}\{A_1 \tan(\gamma_0+\varphi_0)+1\}\right] & \dfrac{2\sqrt{1+\xi_1^2}}{\xi_1 - A_1}\left[-\dfrac{x_1}{u_0} - \dfrac{v_0}{g}\{A_1 \tan(\gamma_0+\varphi_0)+1\}\right] \\ \dfrac{2}{1+A_1^2}\left\{ \dfrac{1}{u_0}\left(-2A_1 + \dfrac{v_0}{u_0}\right) + \dfrac{1}{u_0}\tan(\gamma_0+\varphi_0)\right\} & \dfrac{2}{1+A_1^2}\left\{ \dfrac{1}{u_0} + \dfrac{v_0}{u_0^2}\tan(\gamma_0+\varphi_0)\right\} \end{pmatrix} + \begin{pmatrix} 0 \\ -\dfrac{1}{1+A_1^2}\dfrac{g}{u_0^2}\Delta x_1 + \kappa(s_1)\Delta s_1 \end{pmatrix}. \tag{A18}$$

After some manipulation of the matrices, we finally obtain the linearized mapping of the generalized Birkhoff coordinate $(\Delta s, \Delta p_s)$ where $p_s \equiv p\sin\varphi$ is the tangential momentum to the floor at the point s,

$$\begin{pmatrix} \Delta s_1 \\ \Delta p_{s_1} \end{pmatrix} = \begin{pmatrix} \dfrac{1}{p_1\cos\varphi_1} & 0 \\ 0 & p_1\cos\varphi_1 \end{pmatrix} \begin{pmatrix} m_{11} & m_{12} \\ m_{21} & m_{22} \end{pmatrix} \begin{pmatrix} p_0\cos\varphi_0 & 0 \\ 0 & \dfrac{1}{p_0\cos\varphi_0} \end{pmatrix} \begin{pmatrix} \Delta s_0 \\ \Delta p_{s_0} \end{pmatrix}, \tag{A19}$$

where

$$m_{11} = \frac{1}{p_0^2}(m^2g^2\tau^2 - p_0^2) + \frac{1}{p_0^2}\left\{ \frac{\kappa(s_0)}{m^2 g}p_0^2 - \sin(\gamma_0+\varphi_0)\right\}\frac{mg\tau}{\cos\varphi_0}(mg\tau\sin\gamma_0 - p_0), \tag{A20}$$

$$m_{12} = \frac{p_0}{m}\tau(mg\tau\sin\gamma_0 - p_0), \tag{A21}$$

$$\begin{aligned} m_{21} = {} & \frac{2m^3g^2\tau}{p_0^2p_1^2} + \frac{m^2g(m^2g^2\tau^2 - p_1^2)}{p_0^3p_1^2}\left\{ \frac{\kappa(s_0)}{m^2g}p_0^2 - \sin(\gamma_0+\varphi_0)\right\}\frac{1}{\cos\varphi_0} + \frac{m^2g(m^2g^2\tau^2 - p_0^2)}{p_0^2p_1^3} \\ & \times\left\{ \frac{\kappa(s_1)}{m^2g}p_1^2 - \sin(\gamma_1+\varphi_1)\right\}\frac{1}{\cos\varphi_1} + \frac{m^3g^2\tau}{p_0^2p_1^3}(mg\tau\sin\gamma_0 - p_0)\left\{ \frac{\kappa(s_0)}{m^2g}p_0^2 - \sin(\gamma_0+\varphi_0)\right\} \\ & \times\left\{ \frac{\kappa(s_1)}{m^2g}p_1^2 - \sin(\gamma_1+\varphi_1)\right\}\frac{1}{\cos\varphi_0}\frac{1}{\cos\varphi_1}, \end{aligned} \tag{A22}$$

and

$$m_{22} = \frac{1}{p_1^2}(m^2g^2\tau^2 - p_1^2) + \frac{p_0}{p_1}\frac{1}{p_1^2}\left\{ \frac{\kappa(s_1)}{m^2g}p_1^2 - \sin(\gamma_1+\varphi_1)\right\}\frac{mg\tau}{\cos\varphi_1}(mg\tau\sin\gamma_1 - p_1). \tag{A23}$$

In the above, we denote the time between the collisions by τ.

One can see the mapping from (s_0, p_{s_0}) to (s_1, p_{s_1}) is area preserving because the absolute value of the determinant of the matrix (m_{ij}) is one while the sign of this determinant depends on the orbit $\mathbf{T}_0'$.

In the following, we will derive the formula of the Lyapunov exponent of the billiard in a constant vertical external field by using the linear stability matrices in Eq. (A19).

The operator R_i defined by the transformation at the time i (or the time of collision with the floor) from the perpendicular components of the position and velocity to the orbit to the respective vertical components is

$$R_i = \begin{pmatrix} -\dfrac{1}{\cos\gamma_i} & 0 \\ \dfrac{m^2g}{p_i}\cos\gamma_i\sin\gamma_i & -\cos\gamma_i \end{pmatrix}, \tag{A24}$$

where γ_i is the angle between the velocity vector of the particle and the horizontal axis, and p_i is the momentum of the particle.

At first, we consider the case of the free flight without collision. The infinitesimal change of the orbit varies the position and velocity from the original orbit in time τ by free flight in a constant vertical field. We define the transforma-

tion of the infinitesimal change of the vertical components of the position and velocity of the particle by the free flight as F_i,

$$F_i=\begin{pmatrix} \dfrac{1}{p_{i+1}\cos\gamma_{i+1}} & 0 \\ 0 & p_{i+1}\cos\gamma_{i+1} \end{pmatrix} \times\begin{pmatrix} 1-\dfrac{m^2g^2\tau^2}{p_i^2} & \dfrac{\tau}{2m}(p_i^2+p_{i+1}^2-m^2g^2\tau^2) \\ -\dfrac{2m^3g^2\tau}{p_i^2p_{i+1}^2} & 1-\dfrac{m^2g^2\tau^2}{p_{i+1}^2} \end{pmatrix} \times\begin{pmatrix} p_i\cos\gamma_i & 0 \\ 0 & \dfrac{1}{p_i\cos\gamma_i} \end{pmatrix}. \tag{A25}$$

Next we consider the effect of the ith collision on the infinitesimal change of the vertical components of the position and velocity of the particle from the original orbit that bounces on the floor with the angle φ_i measured from the outer normal vector of the floor. The curvature κ_i of the floor plays a very important role of increasing the separation of the nearby orbits although the motion of the particle could be unstable even on the flat floor in the case of the presence of a vertical external field. The infinitesimal change of the collision results in the transformation C_i that operates the perpendicular components of the position and velocity to the orbit:

$$C_i=\begin{pmatrix} -1 & 0 \\ -\dfrac{2m^2g}{p_i}\left\{\dfrac{\kappa_i}{m^2g}p_i^2-\sin\alpha_i\sin^2\varphi_i\right\}\dfrac{1}{\cos\varphi_i} & -1 \end{pmatrix}, \tag{A26}$$

where α_i denotes the angle between the outer normal to the floor and the horizontal line. Consequently, one can obtain the transformation of the vertical coordinate by the infinitesimal change of the collision,

$$R_iC_iR_i^{-1}=\begin{pmatrix} \dfrac{1}{p_i\cos\gamma_i} & 0 \\ 0 & p_i\cos\gamma_i \end{pmatrix} \times\begin{pmatrix} -1 & 0 \\ -\dfrac{2m^2g}{p_i^3}\left\{\dfrac{\kappa_i}{m^2g}p_i^2-\sin\alpha_i\right\}\dfrac{1}{\cos\varphi_i} & -1 \end{pmatrix} \times\begin{pmatrix} p_i\cos\gamma_i' & 0 \\ 0 & \dfrac{1}{p_i\cos\gamma_i'} \end{pmatrix}, \tag{A27}$$

where γ' is defined as the angle between the orbit before the ith collision and the horizontal axis, i.e.,

$$\gamma_i'=\gamma_i+2\varphi_i-\pi. \tag{A28}$$

From Eqs. (A25) and (A27), we obtain the transformation of the infinitesimal change of the vertical coordinate due to the infinitesimal change of the orbit of the ith collision and successive free flight just before the $(i+1)$th collision,

$$F_iR_iC_iR_i^{-1}=\begin{pmatrix} \dfrac{1}{p_{i+1}\cos\gamma_{i+1}'} & 0 \\ 0 & p_i\cos\gamma_{i+1}' \end{pmatrix} \times\begin{pmatrix} 1-\dfrac{m^2g^2\tau^2}{p_i^2} & \dfrac{\tau}{2m}(p_i^2+p_{i+1}^2-m^2g^2\tau^2) \\ -\dfrac{2m^3g^2\tau}{p_i^2p_{i+1}^2} & 1-\dfrac{m^2g^2\tau^2}{p_{i+1}^2} \end{pmatrix} \times\begin{pmatrix} -1 & 0 \\ -\dfrac{2m^2g}{p_i^3}\left\{\dfrac{\kappa_i}{m^2g}p_i^2-\sin\alpha_i\right\}\dfrac{1}{\cos\varphi_i} & -1 \end{pmatrix} \times\begin{pmatrix} p_i\cos\gamma_i' & 0 \\ 0 & \dfrac{1}{p_i\cos\gamma_i'} \end{pmatrix}. \tag{A29}$$

In the case that the particle collides with the floor successively at the time t_{n-1} and t_n, where $(n-1)$ and n denote the $(n-1)$th and nth collision respectively, from Eq. (A29), one can obtain the relation between the infinitesimal shift $\delta q_v(t_n)$ at time t_n and $\delta q_v(t_{n-1})$ at time t_{n-1} of the perpendicular component of th position of the particle,

$$\begin{aligned}\delta q_v(t_n)&=\delta q_v(t_{n-1}+\tau_{n-1})\\ &=\left\{\left(1-\frac{m^2g^2\tau_{n-1}^2}{p_{n-1}^2}\right)+\frac{\tau_{n-1}}{2}\right.\\ &\quad\left.\times\frac{p_{n-1}^2+p_n^2-m^2g^2\tau_{n-1}^2}{p_{n-1}^2}B_v^{(+)}(n-1)\right\}\delta q_v(t_{n-1}).\end{aligned} \tag{A30}$$

Here the quantity $B_v^{(+)}(n)$ is given by recursion according to the following continuous fraction,

$$B_v^{(+)}(n)=\frac{2mg}{p_n\cos\varphi_n}\left(\frac{\kappa_n}{m^2g}p_n^2-\sin\alpha_n\right)+\frac{1-\dfrac{m^2g^2\tau_{n-1}^2}{p_{n-1}^2}}{\tau_{n-1}\dfrac{p_{n-1}^2+p_n^2-m^2g^2\tau_{n-1}^2}{2p_n^2}-\dfrac{1}{\dfrac{2m^2g^2\tau_{n-1}}{p_{n-1}^2}-\left(1-\dfrac{m^2g^2\tau_{n-1}^2}{p_{n-1}^2}\right)B_v^{(+)}(n-1)}}. \tag{A31}$$

Since the Lyapunov exponent λ is the average rate of exponential separation between trajectories issued from arbitrarily close initial conditions, one can finally obtain the formula (4) for the Lyapunov exponents of the particle bouncing on the floor in a constant vertical external field.

[1] L. A. Bunimovich and Ya. G. Sinai, Commun. Math. Phys. **78**, 247 (1980); *ibid.* **78**, 479 (1981).
[2] P. Gaspard and G. Nicolis, Phys. Rev. Lett. **65**, 1693 (1990).
[3] P. Gaspard, J. Stat. Phys. **68**, 673 (1992).
[4] T. Gilbert, J. R. Dorfman, and P. Gaspard, Nonlinearity **14**, 339 (2001).
[5] P. Gaspard, I. Claus, T. Gilbert, and J. R. Dorfman, Phys. Rev. Lett. **86**, 1506 (2001).
[6] R. Klages and J. R. Dorfman, Phys. Rev. Lett. **74**, 387 (1995); Phys. Rev. E **59**, 5361 (1999).
[7] R. Klages, *Deterministic Diffusion in One-Dimensional Chaotic Dynamical Systems* (Wissenschaft & Technik Verlag, Berlin, 1996).
[8] J. R. Dorfman, *An Introduction to Chaos in Nonequilibrium Statistical Mechanics* (Cambridge University Press, Cambridge, UK, 1999).
[9] P. Gaspard and R. Klages, Chaos **8**, 409 (1998).
[10] A. B. Rechester and R. B. White, Phys. Rev. Lett. **44**, 1586 (1980).
[11] H. E. Lehtihet and B. N. Miller, Physica D **21**, 94 (1986).
[12] M. P. Wojtkowski, Commun. Math. Phys. **126**, 507 (1990); **127**, 425 (1990).
[13] P. Gaspard, *Chaos, Scattering and Statistical Mechanics* (Cambridge University Press, Cambridge, UK, 1998).
[14] P. Gaspard, Phys. Rev. E **53**, 4379 (1996).
[15] G. A. Edgar, Editor, *Classics on Fractals* (Addison-Wesley, Reading, MA, 1993).
[16] R. Klages and J. R. Dorfman, Phys. Rev. E **55**, R1247 (1997).
[17] M. Hénon, Physica D **33**, 132 (1988).
[18] D. Ruelle, *Thermodynamic Formalism* (Addison-Wesley, Reading, MA, 1978).